

Proton-induced fission of ^{181}Ta at high excitation energies

Y. Ayyad,^{1,*} J. Benlliure,¹ E. Casarejos,^{1,†} H. Álvarez-Pol,¹ A. Bacquias,² A. Boudard,³ M. Caamaño,¹ T. Enqvist,⁴ V. Föhr,² A. Kelić-Heil,² K. Kezzar,³ S. Leray,³ D. Mancusi,³ C. Paradela,¹ D. Pérez-Loureiro,¹ R. Pleskač,² J. L. Rodríguez-Sánchez,¹ and D. Tarrío¹

¹*Universidade de Santiago de Compostela, E-15782 Santiago de Compostela, Spain*

²*GSI Helmholtzzentrum für Schwerionenforschung GmbH, Planckstrasse, 1 D-64291 Darmstadt, Germany*

³*CEA-Saclay/IRFU, F-91191 Gif-sur-Ivette, France*

⁴*Oulu Southern Institute and Department of Physics, University of Oulu, FIN-86801, Finland*

(Received 23 December 2013; revised manuscript received 19 March 2014; published 14 May 2014)

Total fission cross sections of ^{181}Ta induced by protons at different relativistic energies have been measured at GSI Darmstadt using the inverse kinematic technique. These data contribute to solve inconsistencies in previously reported measurements, but also help to benchmark state-of-the-art reaction codes. The energy range covered with these measurements allowed us to investigate the onset and temperature dependence of dissipative and transient effects at small deformation.

DOI: [10.1103/PhysRevC.89.054610](https://doi.org/10.1103/PhysRevC.89.054610)

PACS number(s): 25.40.Sc, 25.85.Ge

I. INTRODUCTION

Spallation reactions induced by relativistic protons on ^{181}Ta lead to excited target remnants with large fission barriers (20–25 MeV) while covering a broad range in excitation energy. The investigation of the fission process under these extreme conditions is expected to provide relevant information on the dynamics of fission at high excitation energies. Nuclear fission is, indeed, a process that demands a complex description of the fissioning nucleus according to its excitation energy, its angular momentum, and the deformation dependence of its potential energy. Moreover, one needs a mechanism describing how the nucleus explores the potential-energy landscape. A first approach for this mechanism was proposed by Bohr and Wheeler [1] from a purely statistical standpoint. In parallel, Kramers [2] introduced a dynamical description of the fission process based on the coupling between internal (excitation energy) and collective (deformation) degrees of freedom through a dissipation parameter. Based on these ideas, Grangé *et al.* [3] went a step further by including a time-dependent solution of the fission width that recently has been analytically formulated [4,5]. According to that approach, the coupling between intrinsic and collective degrees of freedom requires a certain transient time-delaying fission with respect to other deexcitation channels. These dynamical effects manifest in a more clear way in fissioning systems with high excitation energy, low angular momentum, and nearly spherical state, as stated in Ref. [6].

Many experimental results have already indicated the role of dissipative and transient effects in fission induced by different reaction mechanisms such as spallation, fragmentation, fusion-fission, or multinucleon transfer. For this purpose, several complementary experimental techniques measuring different observables as signatures of dissipative effects have

been utilized. Some examples are nuclear and atomic clocks that yield information about ground-to-scission times involved in fission. In the former the number of emitted light-particles before fission [7,8], namely neutrons and γ rays [9], are measured, yielding valuable information about fission time scales prior to scission. Two methods involving atomic clocks have been widely used: the filling of the K -shell hole created via the collision of a nuclei with the inner electrons of an atom of a given medium [10] and the crystal blocking technique [11]. In the latter, the measured angular distribution of fission fragments emitted inside a crystal gives information about the scission time. Evaporation and fission cross sections also have been investigated to extract information about pre-saddle dynamical effects on the fission process [12]. A detailed description and compilation of many of these techniques and results can be found in Ref. [13].

These experimental evidences also indicate that transient effects in fission manifest with stronger signatures in fission at high excitation energies [14–17]. However, a precise experimental determination of the onset of these effects with the energy of the fissioning system is still required to better constrain the strength of the nuclear dissipation. However, the temperature dependence of the nuclear viscosity is another subject of controversy. While some authors claim there is a strong dependence of the dissipation strength with temperature [18], other theoretical [19] and experimental works [14] do not observe any evidence for such a dependence or very little.

Tantalum fissioning is of importance not only for basic research, but also for applications. Tantalum and tungsten alloys are also proposed as optimum materials for the construction of spallation neutron sources [20] because of their properties under extreme irradiation conditions: relatively large neutron production, corrosion resistance, and high melting point. Spallation targets are also of interest for accelerator-driven systems (ADS) [21] and for the production of exotic nuclei at facilities such as the isotope separator on-line (ISOLDE) at CERN [22] and neutrinos [23].

To contribute to these questions, in this work we propose to investigate the fission of ^{181}Ta induced by protons covering a

*yassid.ayyad@rcnp.osaka-u.ac.jp

[†]Present address: Escola de Engenharia Industrial, Universidade de Vigo, E-36310 Vigo, Spain.

large energy range, 300 to 1000 MeV. Several arguments supported this choice. Spallation-induced reactions fulfill the conditions for the investigation of dissipative and transient effects: high excitation energies, small initial deformations, and low angular momentum induced by the reaction [6,24]. The large fission barriers in tantalum also help in suppressing low-energy fissions dominated by a quasistationary decay rate. Moreover, because spallation and fragmentation reactions lead to fissioning systems with nearly undistorted shapes [14], comparisons between fission in tantalum (quadrupole deformation parameter $\beta_2 = 0.269$) and in other spherical nuclei, such as lead, may provide some hints about the role of the initial deformation or fissility in the manifestation of transient effects [25]. Finally, the large range of excitation energy covered in these measurements will contribute to the investigation of the onset of transient effects and possible temperature dependence of the dissipation strength. At present, the measurement of the excitation energy in the fission process is a complicated task. However, it can be estimated with realistic reaction-model calculations.

Presently available data related to total fission cross sections of ^{181}Ta above 700 MeV proton-beam energy are scarce and show clear discrepancies at 1000 MeV [26,27]. The situation does not improve at lower energies, where the available data are more abundant, but they also present inconsistent results [28–31], in particular between 300 and 500 MeV. Most of these experiments were performed using passive track detectors and only few of them are based on coincident measurements of both fission fragments [32]. Under such conditions it seems difficult to unambiguously identify a fission channel with a few-mb cross section, as is expected in this case.

All previous measurements of fission reactions induced by protons on ^{181}Ta were performed using the direct kinematics technique. Therefore, the reaction products had very low kinetic energy and in some cases were even stopped in the target material. To overcome this difficulty the inverse kinematics technique was utilized in the present work. Several experiments performed at the FRS (Fragment Separator) spectrometer using the inverse kinematics technique [17,33–37] measured the mass and charge of fission residues with high precision, in addition to the fission cross sections. However, the transmission of the fission fragments was limited by the acceptance of the spectrometer, and only one of the two fission fragments was measured. Therefore, a dedicated experimental setup was used in the present work to register both fission fragments in coincidence with high efficiency and resolution [38].

In this work, we present the results of the experiment performed at GSI (Helmholtzzentrum für Schwerionenforschung) aimed at measuring the total fission cross section of ^{181}Ta induced by protons in the energy range between 300 and 1000 MeV, taking advantage of the inverse kinematics. The dedicated experimental setup made possible the measurement of the cross sections with high precision. State-of-the-art model calculations are benchmarked and used to investigate the influence of dynamical effects in fission.

II. EXPERIMENTAL SETUP

In the present experiment, the ^{181}Ta nuclei were accelerated using the facilities of GSI, the Universal Linear Accelerator

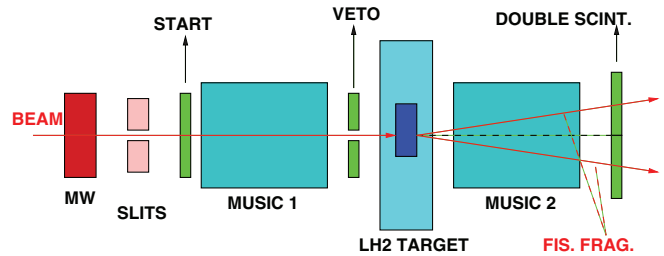


FIG. 1. (Color online) Schematic representation of the experimental setup used in the present experiment.

(UNILAC) and the heavy-ion synchrotron (SIS-18), up to 300, 500, 800, and 1000 A MeV with an intensity of the order of 10^4 ions/s and a spill duration of 7 s. These beams impinged onto a liquid hydrogen target. Owing to the kinematics of the reaction, we were able to detect efficiently both fission fragments which were emitted in the forward direction with large kinetic energies. This experimental approach made possible the use of relatively thick targets, increasing the statistics.

A sketch of the setup is shown in Fig. 1. A multiwire (MW) chamber and thick iron slits were used to position and collimate the ^{181}Ta beam at the target. A first scintillator detector (start) placed upstream of the target, determined the beam flux. The target consisted of a liquid hydrogen cell (85 mg/cm^2) inside a container with $100\text{-}\mu\text{m}$ titanium windows and a cryostat for liquefying the hydrogen. The target was surrounded by two multisampling ionization chambers (MUSICs) [39] ($200 \times 80\text{-mm}$ window surface and 460 mm active length) filled with tetrafluoromethane (CF_4), which measured the energy loss of the tantalum beam particles and that of the products of the reaction, respectively. These ionization chambers, having almost 100% efficiency for the detection of relativistic heavy nuclei, were used to identify reactions of ^{181}Ta produced in the hydrogen target and in any other layer of matter present in the beamline. A veto scintillator with a 15-mm-diameter hole, placed just before the target, allowed the rejection of beam-halo particles and misaligned beam trajectories. The two fission fragments were detected independently, but in temporal coincidence, by a double-paddle scintillator placed downstream of the target (each paddle measuring $300 \times 70 \text{ mm}$ with 3 mm thickness).

According to the setup geometry, two different triggers were used for data acquisition: The “beam” trigger was provided by the plastic scintillator placed upstream of the target in anticoincidence with the signal of the veto scintillator. The “reaction” trigger was produced by the coincidence between the beam trigger and the time-coincident signals on both paddles of the double scintillator placed downstream the target. These two triggers provided the measurement of the beam flux together with the fission events. The average rates for the beam and reaction triggers were around 10^4 and 700 triggers/s, respectively. The beam trigger was downscaled to reduce the data-acquisition dead time.

III. DATA ANALYSIS

The identification of the fission events was based on the amplitude of the signals recorded by the two MUSIC chambers

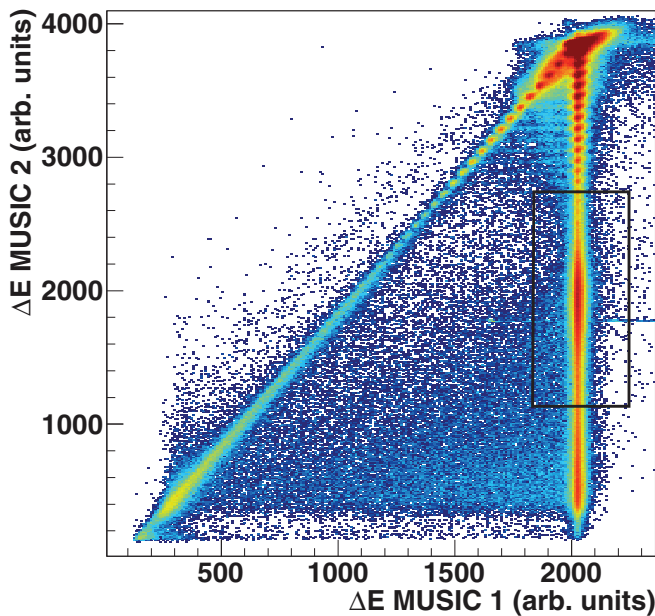


FIG. 2. (Color online) Scatter plot of the amplitudes of the signals registered with the two MUSIC detectors. Nuclei lighter than ^{181}Ta produced in reactions before MUSIC 1 appear in the diagonal region. In the vertical line the ^{181}Ta spot corresponding to noninteracting beam particles is represented, and below are the events corresponding to reactions in the target. The box encloses the fission region and the color code represents counts on a logarithmic scale.

surrounding the target and the amplitude of the signals provided by the two paddles of the double plastic scintillator located downstream of the target. With this information, we were able to isolate fission events from other reaction channels occurring in the hydrogen target.

In Fig. 2 we depict in a scatter plot the energy losses of ions traversing the two MUSICs, before and after the target, obtained with the reaction trigger. The events lying in the diagonal of this plot correspond to ions that kept their atomic number when passing through the target. These nuclei, lighter than the primary beam, have been produced in nuclear reactions induced by ^{181}Ta projectiles in the layers of matter situated upstream of the hydrogen target. The dominant ^{181}Ta spot of noninteracting beam particles is clearly visible at the top, near channel 3800 on the vertical axis. The vertical group, below the beam spot, corresponds to residual fragments produced in the interaction of ^{181}Ta with hydrogen. In this group, events inducing high and small energy-loss signals, correspond to residual heavy nuclei and light nuclei emitted during the deexcitation process.

Because the energy loss of nuclei is proportional to their atomic number squared (Z^2), fission fragments are expected to produce energy-loss signals corresponding to about half of the value obtained for the primary beam ($\Delta E_{\text{f.f.}} \propto Z_1^2 + Z_2^2 = Z_{\text{beam}}^2/2$). Therefore, fission products should be located around channel 1800 on the MUSIC 2 energy-loss axis. To count for the fission events, n_{fiss} , a condition in the scatter plot shown in Fig. 2 was applied selecting the region where

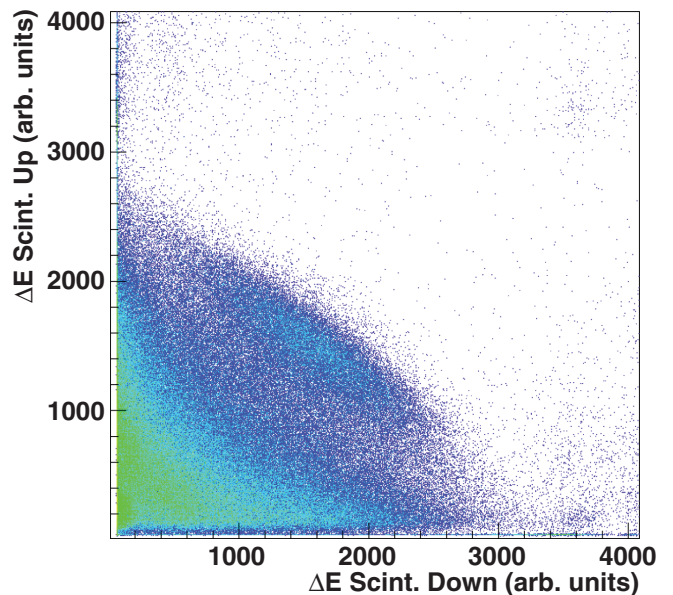
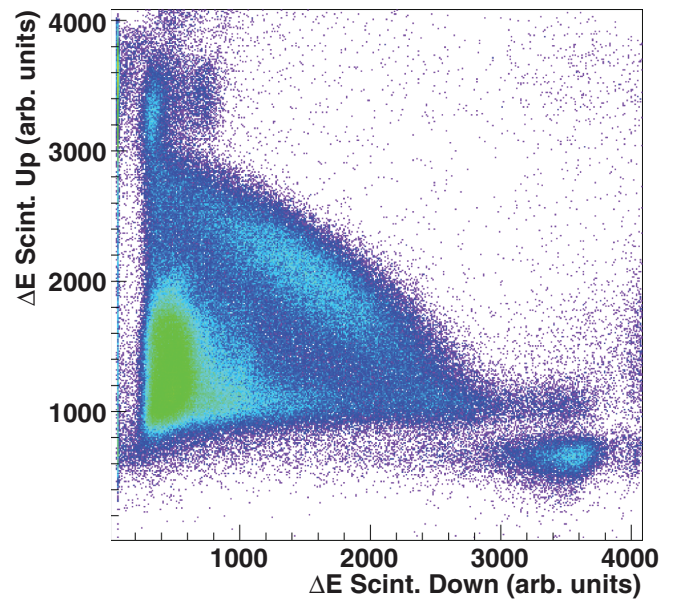


FIG. 3. (Color online) Scatter plot of the energy-loss signals provided by the two paddles of the double plastic scintillator placed downstream from the target with the reaction trigger (top panel, 1 A GeV, full target; bottom panel, 300 A MeV, full target). Both plots are normalized to the same number of counts to highlight the influence of different reaction channels. The color code represents counts on a logarithmic scale.

the fission products are expected. Focusing on the selected region, indicated by the rectangular area in Fig. 2, the fission events were identified combining the amplitude (energy loss) of the signals recorded by the two paddles of the double plastic scintillator.

In Fig. 3 the amplitudes of the signals registered by both plastic scintillators in temporal coincidence (at 1 A GeV in the top panel and 300 A MeV bottom panel), using the reaction trigger, are represented in a scatter plot. Owing to the charge splitting of the fission process, fission events are

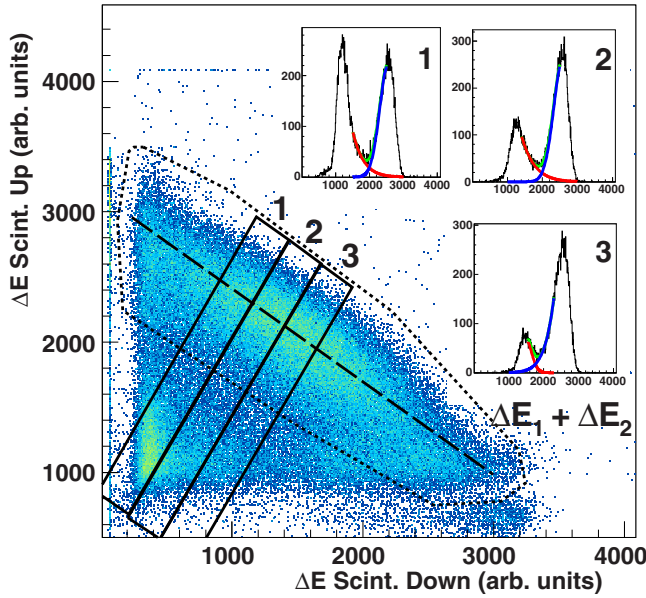


FIG. 4. (Color online) Same as the top panel in Fig. 3 but conditioned by the fission selection from Fig. 2. The different contours and insets illustrate the background suppression method used to identify fission events as explained in the text.

expected to populate the diagonal band defined by a constant value of $Z_1 + Z_2$ in this figure and are separated from other more abundant reaction channels. This fission region only represents a small fraction of the plot statistics because the fission probability is rather small. For this reason, fission events could only be properly identified by a detection setup enabling the identification of different reaction channels.

To provide an accurate measurement of the fission cross section, we evaluated the background which remains in the fission region owing to simultaneous breakup and evaporation processes. To evaluate this background we used Fig. 4, where the energy loss provided by the two paddles for the double plastic scintillator at 1000 A MeV is represented by selecting only events compatible with a fission signal in the MUSIC detectors (rectangular area in Fig. 2).

In this figure, intermediate-mass fragments (IMFs) produced in simultaneous breakup reactions may populate the fission region (dotted contour in Fig. 4). The evaluation of this breakup background was performed via dividing the fission region into slices as shown by the thin rectangles in Fig. 4. Each slice was then projected along its longitudinal dimension (insets in Fig. 4), which clearly enhanced the profile of the contributions coming from background (left peak) and fission (right peak). Gaussian fits to each of the two components defined the correction for the breakup background suppression. However, evaporation residues could also populate the edges of the fission region along an axis $\Delta E_1 + \Delta E_2$ (dashed line in Fig. 4) defined by the sum of the signals of the two scintillators. To overcome this problem, the region profile (dotted contour in Fig. 4) was projected onto this $\Delta E_1 + \Delta E_2$ axis to evaluate this contribution by means of Gaussian fits, as shown in Fig. 5.

The number of measured fission events n_{fiss} corresponds then to the number of events in the fission region corrected by

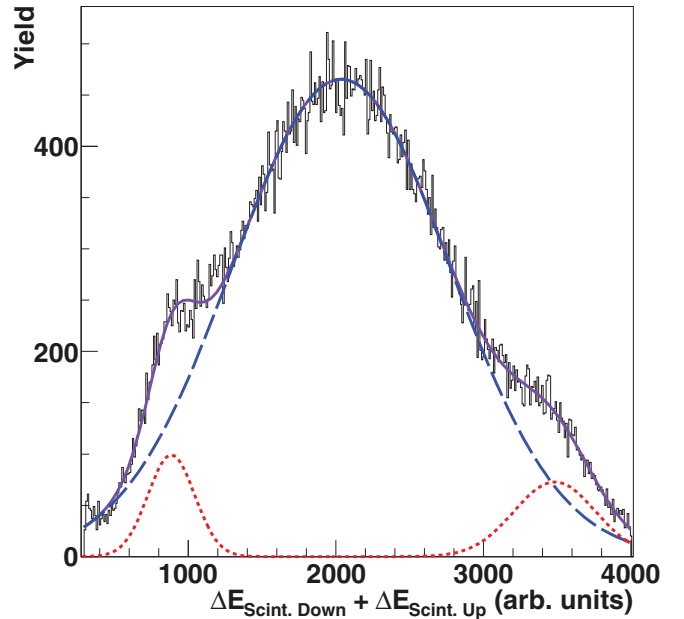


FIG. 5. (Color online) Projection of the fission region defined in Fig. 4 on the $\Delta E_1 + \Delta E_2$ axis represented in the same figure. The contribution of evaporation residues was evaluated by means of a Gaussian fit (dotted line) and subtracted from the total contribution (solid line).

background contributions produced by particle evaporation or simultaneous breakup.

Fission yields (Y_{fiss}) were obtained from fission-event measurements corrected by the background (n_{fiss}) and additional effects such as the secondary reactions of the fragments in the target (ε_d) and the geometrical acceptance of the experimental setup (ε_{geo}), according to the equation

$$Y_{\text{fiss}} = n_{\text{fiss}} f_d f_{\text{geo}}, \quad (1)$$

where $f_d = 1/(1 - \varepsilon_d)$ and $f_{\text{geo}} = 1/\varepsilon_{\text{geo}}$.

Secondary reactions of the fission fragments (ε_d) in the target were evaluated by calculating the inverse of the survival probability inside the target and in consecutive layers,

$$P(Z, A) = \prod_i e^{\sigma_T^i(Z, A) x_i}, \quad (2)$$

where $\sigma_T^i(Z, A)$ is the total reaction cross section and x_i is the density of atoms per unit area of the layer. The fission fragment distribution was estimated with nuclear-reaction codes (see Sec. V B). The reaction cross sections were calculated using Karol's microscopic model [40]. The correction amounted to less than 2.5% for full target and less than 0.5% for empty target measurements at 1000 A MeV. Geometrical constraints were also considered to evaluate the geometrical efficiency of the detection setup. Fission products emitted close to the horizontal plane were detected with a smaller efficiency because of the separation gap between the two plastic scintillators (around 1 mm) and the possibility that both fragments traverse the same paddle because of the beam spread and alignment. A Monte Carlo simulation based on the Wilkins formula for calculation of the postscission

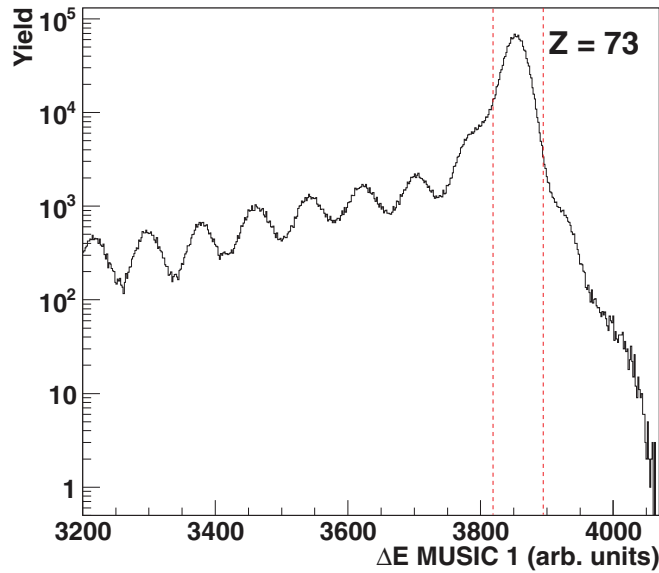


FIG. 6. (Color online) Energy-loss signals provided by MUSIC 1. The region between the dotted red lines corresponds to ^{181}Ta .

kinetic energy of the fission fragments [41] was performed to evaluate the losses owing to the geometrical constraints of the setup. Taking into account the dispersion of the beam, as measured with the MW chamber detector and the alignment, the Coulomb force between both fragments and the distance from the center of the hydrogen target to the double plastic scintillator, we calculated the perpendicular dimensions of the fission fragment distribution in the double plastic scintillator detection plane. The resulting correction ϵ_{geo} is of the order of 91% at 1000 A MeV and around 95% at 300 A MeV.

To determine the number of projectiles (n_b), we used the first MUSIC to identify tantalum among other nuclei that have been created in other layers of matter placed in the beamline before the target, as shown in Fig. 6. The amount of $Z = 73$ ions identified according to this procedure using the beam and the reaction triggers corrected by the downscaling factor provided the total number of projectiles.

Owing to the relatively large thickness of the target, the attenuation of the beam was considered applying a correction factor ϵ_a . This correction factor, evaluated with Karol's formula, amounted to around 5% for the full target and less than 1% for the empty target.

TABLE I. Statistical ($\epsilon_{\text{stat.}}$) and systematic uncertainties owing to the identification of fission fragments [$\epsilon(n_{\text{fiss}})$], geometrical acceptance [$\epsilon(\epsilon_{\text{geo}})$], attenuation of the beam [$\epsilon(\epsilon_a)$], and secondary reactions [$\epsilon(\epsilon_d)$] affecting our measurements.

Energy (A MeV)	$\epsilon_{\text{stat.}}$ (%)	$\epsilon(n_{\text{fiss}})$ (%)	$\epsilon(\epsilon_{\text{geo}})$ (%)	$\epsilon(\epsilon_a)$ (%)	$\epsilon(\epsilon_d)$ (%)
1000	0.38	6.01	4.32	0.43	0.22
800	0.39	7.16	3.72	0.41	0.22
500	0.45	7.84	2.80	0.39	0.22
300	0.33	9.51	2.05	0.38	0.22

TABLE II. Same as Table I but for empty target measurements.

Energy (A MeV)	$\epsilon_{\text{stat.}}$ (%)	$\epsilon(n_{\text{fiss}})$ (%)	$\epsilon(\epsilon_{\text{geo}})$ (%)	$\epsilon(\epsilon_a)$ (%)	$\epsilon(\epsilon_d)$ (%)
1000	1.45	1.95	4.32	0.05	0.04
800	1.05	4.56	3.72	0.05	0.04
500 ^a	–	6.71	2.80	0.05	0.04
300	0.96	7.08	2.05	0.05	0.04

^aAt 500 A MeV the background produced by reactions in the liquid hydrogen container could not be measured and was estimated using a parametrization of the normalized yields at other energies based on Prokofiev systematics.

To consider reactions taking place in the target windows (namely Ti), fission yields measured with the empty target were subtracted from the fission yields obtained with the full target. Finally, the respective fission yields were normalized to the number of projectiles and the number of nuclei in the target per surface unit (N_t) to determine the total fission cross section according to the following expression (with $N_b = n_b f_a$ and $f_a = 1 - \epsilon_d$):

$$\sigma = \left(\frac{Y_{\text{fiss}}^{\text{full}}}{N_b^{\text{full}}} - \frac{Y_{\text{fiss}}^{\text{empty}}}{N_b^{\text{empty}}} \right) \frac{1}{N_t}. \quad (3)$$

In these measurements, the main sources of systematic uncertainties were the identification of fission events ranging from 2% to 10% [$\epsilon(n_{\text{fiss}})$], the beam intensity ($\approx 5\%$), and the target thickness ($\approx 4\%$). The sources of systematic uncertainty for the different correction factors were also evaluated. The systematic uncertainty of the geometrical correction factor (ϵ_{geo}) was estimated to be smaller than 5%. The evaluation was done by changing the size of the double plastic scintillator gap and the beam profile in our simulation. The value of the systematic uncertainty of the correction factors owing to the beam attenuation (ϵ_a) and the secondary reactions of the fission fragments (ϵ_d) were smaller than 1% and almost the same for all energies. Owing to the relatively large number of recorded fission events the statistical uncertainties were below 1.5%. Statistical and systematic uncertainties, other than the ones associated with the beam intensity and target thickness, for the measurements with the full and empty target are presented in Tables I and II.

IV. RESULTS

Using the method described in the previous sections, we have measured with high precision the total fission cross section of ^{181}Ta impinging protons at 300, 500, 800, and 1000 A MeV. The results obtained for each energy are presented in Table III. The magnitude of the measured cross sections is rather small and strongly decreases for the lower beam energies. The associated uncertainties are also rather small ($\approx 10\%$) but increase for the lowest energies ($\approx 18\%$) because the smaller fission cross sections complicate the identification of fission events.

In Fig. 7, we present the cross sections obtained in this work as solid points compared to previous measurements obtained by different authors. In this figure, we also present predictions

TABLE III. Total fission cross sections determined in this work.

Energy (A MeV)	Fission cross section (mb)	Statistical uncertainty (%)	System uncertainty (%)
1000	20.17 ± 2.19	0.46	10.85
800	13.09 ± 1.62	0.32	12.34
500	7.53 ± 1.40	0.51	18.54
300	6.55 ± 1.00	0.48	15.21

obtained with the systematics established by Prokofiev some years ago [42] (dashed line).

From the analysis of the previously measured cross sections, one can identify some clear discrepancies. At the highest energies, one can find two rather discrepant measurements around 670 MeV by Konshin *et al.* [29] (14.0 ± 1.9 mb) and by Baranovskiy *et al.* [28] (8.0 ± 2.5 mb). At 800 MeV there is a single measurement by Yurevich *et al.* [26] and at 1000 MeV one finds again two discrepant values obtained by Yurevich *et al.* (15.65 ± 5.4 mb) and Bochagov *et al.* [27] (27.0 ± 1.5 mb). Our results are in very good agreement with the measurement of Yurevich *et al.* at 800 MeV and within the error bars at 1000 MeV, solving the existing discrepancy in this energy range. Moreover, we also confirm the predictions estimated by the systematics of Prokofiev.

In the energy range between 300 and 600 MeV, we can also observe important discrepancies between different measurements. Around 300 MeV the data obtained by Yurevich *et al.* (5.2 ± 1.6 mb) and Konshin *et al.* (2.6 ± 0.4 mb) differ by a factor two, while at 400 MeV both measurements are in good agreement (Yurevich, 5.79 ± 1.78 mb; Konshin, 4.7 ± 0.7 mb). The measurement by Konshin *et al.* is significantly smaller than the one obtained from the systematics of Prokofiev at 400 MeV (7.60 mb). The measurement by Yurevich *et al.* could be compatible with the systematics

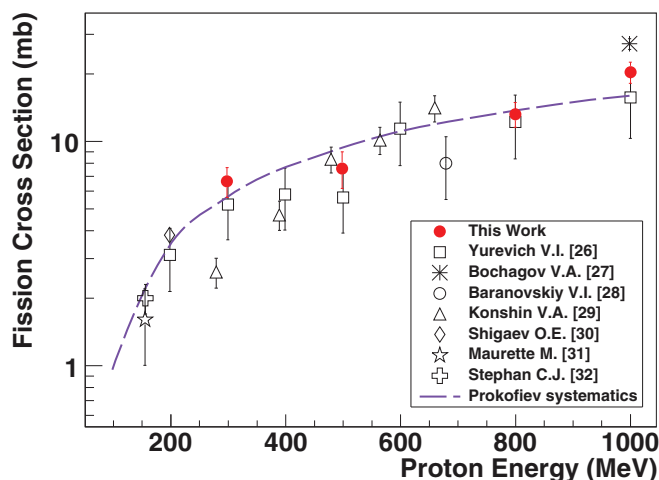


FIG. 7. (Color online) Fission cross sections measured in this work (solid circles) in comparison to previously measured data and estimates obtained from the systematics established by Prokofiev (dashed line).

owing to its large uncertainty. Finally, around 500 MeV the measurements by Konshin *et al.* (8.3 ± 1.1 mb) and Yurevich *et al.* (5.59 ± 1.72 mb) also differ by a large factor but are consistent within the error bars. Our measurements at 300 and 500 MeV are consistent with the estimated values from the Prokofiev formula and confirm the largest values of the cross sections measured in this region.

From this analysis we can conclude that our data confirm the measurements by Yurevich *et al.* above 700 MeV. At lower energies our measurements clarify the discrepancies existing until now. In the energy range between 300 and 600 MeV, our data favor those measurements presenting the highest cross sections. Moreover, our data confirm the predictions obtained by the systematics of Prokofiev over the entire energy range covered by this work.

V. FISSION DYNAMICS AT HIGH EXCITATION ENERGY

The data obtained in this work fulfill the conditions for the investigation of dissipative and transient effects in fission; however, dissipative and transient effects in nuclear fission cannot be directly measured. Therefore, one needs appropriate observables and model calculations providing the link between those observables and the parameters describing the fission dynamics. In the following we detail state-of-the-art reaction codes used to describe these reactions and we benchmark them with the data measured in this work.

A. Description of model calculations

In this work we have used a two-stage approach to describe spallation-induced fission reactions. Intranuclear cascade models allow us to describe the interaction between the proton and the ^{181}Ta nucleus, leading to a remnant in thermal equilibrium. In a second stage deexcitation codes are used to describe the fission process.

For the first stage two different intranuclear-cascade models were used: INCL4.6 (Liège) [43,44] and ISABEL [45]. The former can be applied to reactions induced by nucleons, pions, or light composite particles from 100 A MeV to 3 A GeV incident energy. Target nuclei are endowed with a realistic phase-space density (Woods-Saxon in configuration space, hard Fermi sphere in momentum space). INCL can be considered to be free from adjustable parameters. Optimal values were chosen once and for all by the authors based on extensive validation of the model predictions for widely different observables in a large range of projectile-target-energy combinations. A peculiar characteristic of INCL is the self-consistent determination of the cascade stopping time.

The interaction between the projectile particles, following relativistic kinematics, and the target nucleus is described as a succession of binary collisions between the nucleons along a complete cascade event. The collision criterion is ruled by the mean-free path of the nucleons defined by nucleon-nucleon cross sections. Pions and Δ resonances are produced in the nucleon-nucleon interaction following the reactions $NN \rightleftharpoons N\Delta$ and $\Delta \rightleftharpoons \pi N$. To reject unphysical situations, Pauli blocking is implemented to avoid the population of occupied

final states. Reflexions and transmission of the participants in the surface of the potential of the target are also considered.

The final excitation energy and angular momentum induced in the system by the intranuclear cascade is determined by particle-hole excitations produced in the initial Fermi distribution of the target. The evolution of every particle in the system is followed as the time evolves and at the end of the cascade process the velocity of all the emitted particles and the characteristics of the remnant nucleus are calculated. The cascade stopping time is determined self-consistently.

The ISABEL model describes nucleon-nucleus and nucleus-nucleus collisions also within a relativistic classical mechanics frame up to 1 A GeV. The description of the intranuclear-cascade process is very similar to that of INCL, so we explain only the main differences. In ISABEL projectile and target nucleons are not described as pointlike particles but as a continuous medium or Fermi sea which is perturbed by the collisions induced by the cascade particles (particles pushed off out of the Fermi sea). Interactions between nucleons in the same Fermi sea (target or the projectile distributions) are not allowed as in INCL.

Another difference with respect to INCL is the nuclear density distributions. In ISABEL, both projectile and target distributions follow a folded Yukawa density distribution approximated by 16 constant-density regions. As the cascade evolves, the Fermi sea is depleted and the nuclear density is readjusted to calculate the evolution of the excited nucleons. In ISABEL the cascade stops when the energy of the cascade particles are below an specific cutoff energy given by the Coulomb barrier plus two times the binding energy. Then the remaining excitation energy is distributed among all the nucleons, producing a thermalized prefragment.

In the deexcitation stage, the fission rate is usually described by the transient-state model of Bohr-Wheeler [1]. In contrast to particle evaporation, where the decay rate depends on the level density of the final state, in the Bohr-Wheeler approach the decay rate is defined by the density of states above the fission barrier (saddle point) and the phase space the fission fragments occupy along the deformation axis. The expression for the fission decay width obtained by Moretto [46] based on the Bohr-Wheeler model is

$$\Gamma_f^{\text{BW}} = \frac{1}{2\pi\rho_{\text{gs}}(E_i)} T_{\text{sad}} \rho_{\text{sad}}(E_i - B_f), \quad (4)$$

with T_{sad} being the nuclear temperature at the saddle point, B_f the fission barrier, and E_i the initial excitation energy. ρ_{gs} and ρ_{sad} are the densities of states at ground deformation and above the barrier, respectively.

Another approach to determine the fission width is based on the Kramers solution of the Fokker-Planck equation (FPE) describing fission as a diffusion process across the barrier, ruled by a dissipation coefficient β [2]. Therefore, according to this picture, fission is a dynamical process where the fission rate can be obtained for the overdamp regime according to

$$\Gamma_f^K = \Gamma_f^{\text{BW}} \left\{ \left[1 + \left(\frac{\beta}{2\omega_0} \right)^2 \right]^{1/2} - \frac{\beta}{2\omega_0} \right\}, \quad (5)$$

where Γ_f^{BW} is the Bohr and Wheeler fission decay width and ω_0 is the frequency of the harmonic oscillator of the inverted potential at the saddle point. β is the reduced dissipation coefficient which represents the excitation energy rate exchange between collective degrees of freedom and the heat bath (intrinsic degrees of freedom).

Later, Grangé *et al.* [3] proposed a time-dependent fission decay width, $\Gamma(t)$, by numerically solving the FPE and considering a spherical system at ground deformation with high intrinsic excitation energy and low angular momentum. According to this solution, during the early stage of the process, $\Gamma(t)$ is completely suppressed and needs a transient time, τ_f , to reach 90% of its asymptotic value, which corresponds to the stationary Kramers fission decay width.

In this work we have used two codes, ABLA07 [47] and GEMINI++ [48], to model the de-excitation process. ABLA07 is a statistical code where the deexcitation of a nucleus emitting γ rays, neutrons, light-charged particles, and IMFs is described according to Weisskopf's model [49]. In the standard version of ABLA, fission is described as a diffusion process across the barrier. In that approach the time-dependent fission width is obtained from an analytical solution of the FPE describing the diffusion [5,24]. Moreover, the effect of the initial deformation of the fissioning system in the fission width is considered according to Ref. [50]. At each deexcitation step, the statistical decay widths for all deexcitation channels are calculated for the corresponding compound nucleus; however, the fission width is obtained from the analytical expression of $\Gamma(t)$ given by the FPE solution. The deexcitation time accumulates along the complete deexcitation chain [5]. As an option, ABLA can also calculate the fission width statistically according to the transition-state model of Bohr and Wheeler, using the formulation proposed by Moretto [46] or using the time-independent solution proposed by Kramers [2].

In all fission models, a critical parameter contributing to the fission width is the ratio of the level-density parameter used in the fission channel to that used in neutron evaporation, a_f/a_n [51–56]. Several parametrizations based on measurements of the resonances produced in neutron capture and proton or α elastic scattering reactions have been used to determine these level-density parameters. In ABLA these parameters are obtained according to the parametrization presented in Ref. [57]. The deformation-dependent level-density parameters are calculated as a function of the mass number A and the ratio between the nuclear surfaces at ground and at saddle deformation (B_s):

$$a = 0.073A + 0.095B_s A^{2/3}. \quad (6)$$

According to Ref. [52,58], the Kramers fission width calculated with Eq. (5) needs to be modified to include the Strutinsky [59] factor accounting for stationary collective states at ground deformation. The effect of including this factor has been suggested to be analog to the use of realistic deformation-dependent level-density parameters [60]. Indeed, the authors of Ref. [14] indicate that the parametrization of the level-density parameter according to Eq. (6) should account for the effect of the Strutinsky factor.

Another relevant parameter affecting the fission width is the description of the fission barrier. ABLA uses angular momentum-dependent fission barriers based on the finite-range liquid-drop model of Sierk [61] considering ground-state shell effects [62]. Therefore, the fission model we used to infer the value of the reduced dissipation parameter fulfills the conditions established by Lestone and McCalla [58], considering the rather low angular momentum induced in spallation reactions.

It should be also emphasized that in ABLA there is an excitation energy threshold above which the prefragment deexcites undergoing breakup or multifragmentation [63]. This limiting excitation energy is fixed at a temperature of 5.5 MeV for all prefragments, as deduced from Natowitz's parametrization [64]. Therefore, very high excitation energy fission events are suppressed by this breakup channel.

GEMINI++ [48,65] is another widely used statistical code also describing the deexcitation process. The evaporation of light-charged particles is described by the Hauser-Feshbach [66] formalism, which includes a more specific angular momentum treatment. The fission probability is calculated numerically, integrating the Bohr-Wheeler width, while IMF emission is predicted using Moretto's [46] formulation as asymmetric-fission events. As is the case with ABLA, fission barriers are also taken from Sierk's model. On the contrary, the ratio of level-density parameter, a_f/a_n , is adjusted to 1.036 [65] to reproduce the experimental data of light-particle kinetic-energy spectra and fission yields.

B. Model benchmarking

In the following we make use of the data measured in this work for benchmarking these model calculations. In Fig. 8 we compare the measured total fission cross sections (points), and the estimated values with the systematic obtained by Prokofiev [42] (crosses), with model predictions obtained with the intranuclear cascade codes INCL and ISABEL coupled to the deexcitation codes ABLA and GEMINI++. In calculations

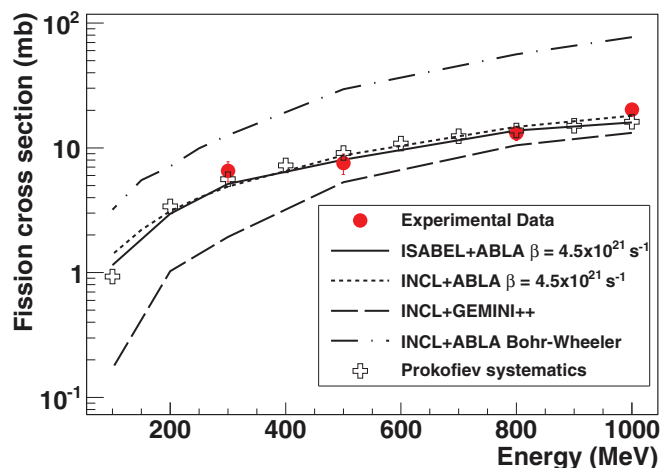


FIG. 8. (Color online) Fission cross sections measured in this work (solid circles) in comparison to model calculations using INCL+ABLA, ISABEL+ABLA, and INCL+GEMINI++.

performed with ABLA we have used the standard version of this code, including a dynamical description of fission based on dissipative and transient effects, as well as a purely statistical version based on the Bohr and Wheeler approach of the fission width.

As can be seen in Fig. 8, results obtained with INCL coupled to the standard version of ABLA with a value of the reduced dissipation parameter $\beta = 4.5 \times 10^{21} \text{ s}^{-1}$ (dotted line) provides a good description of the measured fission cross sections along the full range of proton energies covered in this work. This result is in agreement with previous works where fission cross sections of preactinides induced by spallation [16,17,67] and fragmentation [14,15] reactions could also be reproduced with the same code and parameters.

We also benchmarked intranuclear cascade codes coupling the standard version of ABLA to INCL (dotted line) and ISABEL (solid line). As can be seen, both cascade codes predict very similar total fission cross sections, in good agreement with the experimental data. Therefore, we can conclude that any difference in the prediction of the fission cross sections will be mostly attributable to the deexcitation model.

Finally, we performed calculations using a purely statistical description of the fission process based in the Bohr-Wheeler approach without considering dissipative effects. In these calculations we coupled the intranuclear cascade INCL to the statistical version of ABLA (dash-dotted line) and to the code GEMINI++ (dashed line). In contrast to the dynamical calculations, the statistical version of ABLA clearly overestimate the fission cross sections for all the proton energies covered by this work. This difference can be understood as a consequence of the hindrance of the fission channel induced by dissipative and transient effects. GEMINI++, using the same Bohr-Wheeler prescription to determine the fission width, provides much smaller fission cross sections underpredicting the measured values.

The difference between these two statistical calculations could be explained in terms of the different parameters used to compute the fission width and other competing channels. Because both codes use the same masses and fission barriers, one of the main difference seems to be on the level densities. As previously stated, the ratio of the level-density parameters at saddle and at ground deformation used in GEMINI++ for the reaction under investigation is fixed to a value $a_f/a_n = 1.036$. However, ABLA determines the level densities at ground and saddle deformation following the well-established prescription by Ignatyuk *et al.* [57]. In this case, the average value of the ratio of the level densities at saddle and at ground deformation is around 1.06. This difference should then contribute to the smaller fission cross sections obtained with GEMINI++. Nevertheless, one also should take into account that the inverse cross sections used to compute particle emission, which play an important role in the fission probability, are different in both codes. In addition, IMF emission is also described according two different formalisms in ABLA and GEMINI++.

Our analysis indicates that calculated fission probabilities depend on, among others, two competing parameters, dissipation and level densities, that cannot be unambiguously fixed with a single observable. The same conclusion was obtained in other works, where additional observables were proposed. In

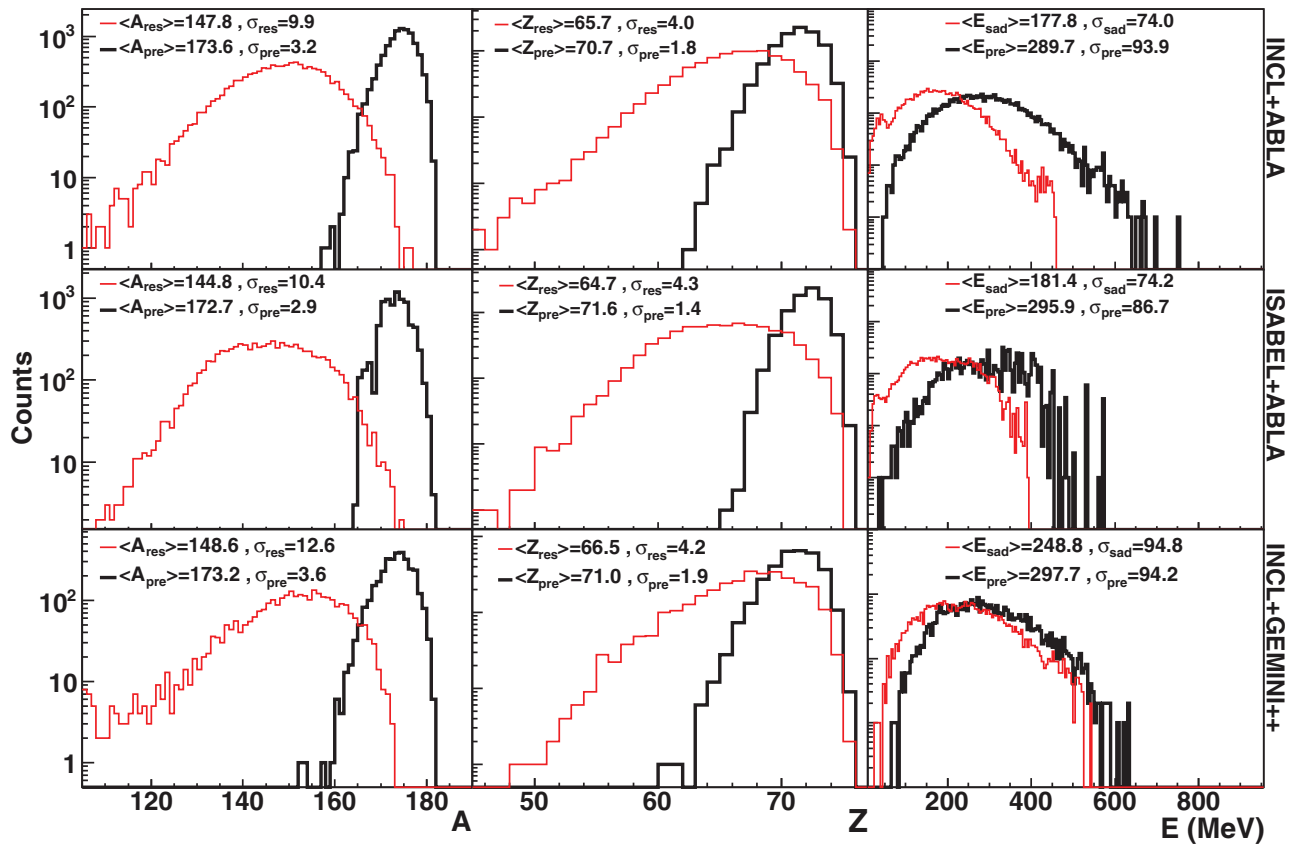


FIG. 9. (Color online) Mass, charge, and excitation energy distributions of the prefragments leading to fission produced at the end of the intranuclear cascade (thick line) and the residual nuclei reconstructed from both fission fragments (thin line) for the reaction $^{181}\text{Ta} + p$ at 1 A GeV, predicted by INCL+GEMINI++, and ISABEL+ABLA, and INCL+ABLA considering $\beta = 4.5 \times 10^{21} \text{ s}^{-1}$. For the excitation energy distributions, the thin line refers to the system at the saddle point.

Refs. [15–17] fission cross sections and the width of the charge distribution of the fission fragments, probing the excitation energy of the fissioning system at saddle, were used. Authors of Ref. [68] proposed as additional observable the excitation energy of the fissioning system at scission, although this information cannot yet be determined experimentally.

In the following we also propose to use our calculations to better understand the differences between these models, using additional observables that could not be measured in the present work. These observables, which could help to evidence the role of dissipative and transient effects are the mass, charge, and excitation energy distributions of nuclei undergoing fission.

In Fig. 9 we present calculations performed with different combinations of the codes used in this work. Predictions obtained with INCL+ABLA, ISABEL+ABLA, and INCL+GEMINI++ are shown in the first, second, and third rows of panels, respectively. ABLA calculations are made according to the dynamical picture of the fission process. Thick and thin lines represent the results of calculations of the mass and atomic number of the fissioning prefragments (A_{pre} and Z_{pre}) as produced by the intranuclear cascade, and the mass and atomic number of the fission residual nuclei reconstructed using the mass and charge of both fission fragments (A_{res} and Z_{res}), respectively. In the case of the excitation energy, the thin

line represents the excitation energy at the saddle point and the thick line describes the initial excitation energy of the prefragment at ground deformation. All these calculations were performed for a kinetic energy of the projectiles of 1 A GeV.

As can be seen in Fig. 9, the mean value of the excitation energy of the prefragments (E_{pre}) is similar for the three calculations. However, dynamical calculations performed with ABLA show a smaller mean value of the excitation energy at the saddle point as compared to GEMINI++. This reduction in the excitation energy is attributable to the cooling by nucleon evaporation during the time delay of fission induced by dissipation.

Relevant information can be also inferred from the mass and atomic number of the residual nuclei reconstructed using the mass and atomic number of the final fission fragments (A_{res} and Z_{res} , thin lines). One can see that calculations with ABLA and GEMINI++ predict similar mass and charge distributions of the final residual nuclei. This result would indicate that the cooling of the hot prefragments follows similar evaporation chains in both codes, the only difference being the moment at which fission takes place. It seems clear that in ABLA a sizable fraction of the evaporated nucleons is emitted by the fissioning nucleus before reaching the saddle point. In contrast, in GEMINI++ most of the nucleons are evaporated after saddle.

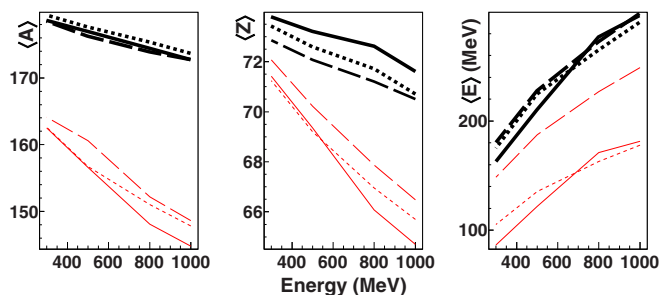


FIG. 10. (Color online) Mean value of the mass, charge, and excitation energy of the prefragments leading to fission (thick lines) and the residual nuclei reconstructed using the mass and atomic number of both fission fragments, A_{res} and Z_{res} (thin lines) for the reaction $^{181}\text{Ta} + p$ as a function of the beam energy calculated with INCL+ABLA (dotted lines) and ISABEL+ABLA (solid lines) considering $\beta = 4.5 \times 10^{21} \text{ s}^{-1}$ and INCL+GEMINI++ (dashed lines). For the excitation energy curves, thin lines refer to the saddle point.

To investigate the energy dependence of the observables shown in Fig. 9, we plotted in Figs. 10 and 11 the mean value and the root mean square (rms) of the distributions as a function of the proton incident energy. As shown in these figures, the evolution of the mean value and rms of the mass, charge, and excitation energy distributions is similar for all the calculations, having a slight deviation in the case of the charge of the residual nuclei calculated with INCL+GEMINI++ that increases with energy. Therefore, all the conclusions we have obtained at 1 A GeV can be applied for the other energies presented here.

Calculations performed with both intranuclear cascade codes, INCL and ISABEL, coupled to ABLA yield consistent values of the fission cross section and similar mass and excitation-energy distributions, but they show some small differences in the mean value and rms of the charge distribution of the prefragments, as shown in in Figs. 10 and 11 (thick lines). Predictions made using ISABEL+ABLA (solid line) show narrower charge distributions with slightly larger mean values. Besides these small differences, we can conclude that the performance of both intranuclear cascade codes is rather similar.

These calculations confirm previous investigations indicating that the combined measurements of fission cross sections and observables sensitive to the excitation energy

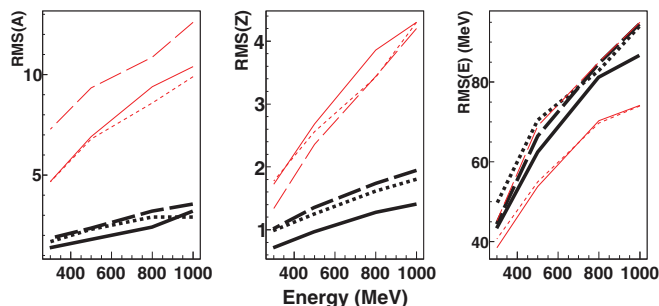


FIG. 11. (Color online) Same as Fig. 10 but for the RMS of the distributions.

of the fissioning system made it possible to unambiguously investigate dissipative and transient effects. In our case, we use a single observable but also a code with parameters that have been proven to correctly describe other observables and reactions [14,15].

C. Dissipative and transient effects

Nowadays, it is well established that fission should be understood as a diffusion process across the fission barrier ruled by dissipation. However, the nature and magnitude of this parameter is still under debate. Moreover, possible dependencies with deformation and temperature, or the presence of transient effects are also discussed.

Measurements at low and moderate excitation energies (up to 120 MeV), mostly based in fusion-fission reactions, use pre- and postscission particle emission to assess the magnitude of the dissipation parameter at small and large deformation. These results are rather discrepant because some authors find a strong deformation dependence [12], while others find a strong temperature dependence [69]. Despite these discrepancies, caused very often by the different model approaches and parameters used to determine the strength of the nuclear viscosity, many results point to a value for this parameter at small deformation around $\beta = 3-7 \times 10^{21} \text{ s}^{-1}$ [12,69-71].

Experiments based on fragmentation or spallation reactions [4,14,16,17], gave access to the production of fissioning systems with higher excitation energies (100 to 500 MeV). These experiments, mostly measuring fission cross sections and the nature of the final fission fragments, confirm the above-mentioned values for the magnitude of the dissipation parameter and transients times at small deformation around $\beta = 1-5 \times 10^{21} \text{ s}^{-1}$.

The measurement of the proton-induced fission on ^{181}Ta at different kinetic energies performed in this work fulfills the optimum conditions required for the manifestation of transient effects [6,24]. The data span a large range in excitation energy. Moreover, the reaction mechanism induces rather low angular momentum. Finally, the low fissility helps suppress low-energy fission, while the initial deformation can be used to test these effects in the dynamics and the determination of transient times [50]. Therefore, these data can be used to investigate the manifestation of transient effects and possible temperature dependencies of the presaddle dissipation strength.

The manifestation of transient effects is still a subject of debate. Experiments using fusion-fission reactions obtain rather different values. Some works do not show any room for transient effects [72,73], while others seem to converge around transient times below $\tau_f = 10^{-20} \text{ s}$ [58,74]. However, these results could be biased by the choice of parameters entering the respective model calculations, in particular, level-density parameters, as discussed in Sec. VB. These small values for the transient time seem to be in agreement with the $\tau_f = 2-5 \times 10^{-21} \text{ s}$ obtained while investigating spallation [16,17] and fragmentation reactions [14,15]. According to this value, transient time will only delay the fission process at excitation energies above 150 MeV. This threshold may explain why fusion-fission reactions are generally insensitive to transient effects.

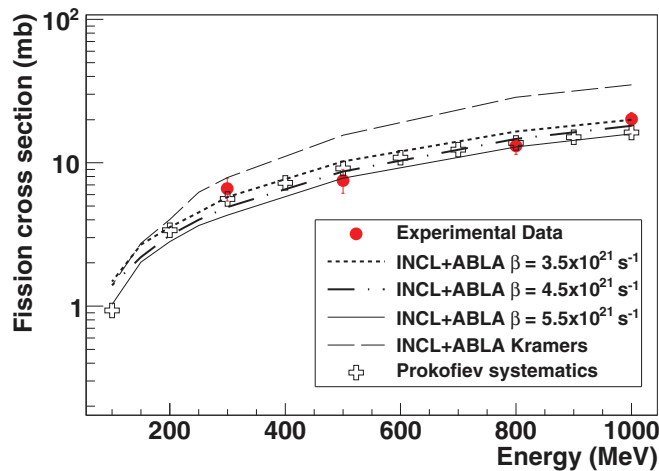


FIG. 12. (Color online) Fission cross sections measured in this work (solid circles) in comparison to calculations using INCL+ABLA for different values of the reduced dissipation coefficient and considering the Kramers picture of fission. The cross sections predicted by the systematics of Prokofiev [42] are indicated by crosses.

In our case, we investigated the manifestation of transient effects by confronting the fission cross sections of ^{181}Ta at different proton energies with calculations using the code ABLA based on a Kramers time-independent fission decay width [2] and calculations with the standard version of the code based on a time-dependent fission decay width according to the formulation proposed in Refs. [4,5].

The results of these calculations are reported in Fig. 12, where the dashed line represents the time-independent calculations with a value of the reduced dissipation parameter of $\beta = 4.5 \times 10^{21} \text{ s}^{-1}$ and the dash-dotted line corresponds to time-dependent calculations with the same value for the reduced dissipation parameter. The average transient time obtained according to Ref. [6] using the value of the viscosity parameter obtained in this work amounts to $\tau_f = 1.0 \pm 0.3 \times 10^{-21} \text{ s}$. By contrast, for the lowest energies both calculations yield similar cross sections up to a proton energy around 250 MeV, which corresponds to an excitation energy of the fissioning system around 100 MeV. This onset of transient effects seems to be in good agreement with the results obtained in fusion-fission and fragmentation-fission reactions previously discussed.

The onset of transient effects can also be illustrated by comparing the simulated fission lifetimes with the corresponding transient times, as shown in Fig. 13 as a function of the proton kinetic energy. Fission lifetimes were obtained by accumulating the decay time along the complete deexcitation chain until the system reaches the saddle point. The same value of the reduced dissipation factor $\beta = 4.5 \times 10^{21} \text{ s}^{-1}$ that reproduces the data measured in this work was used to evaluate the fission width and the transient time. The fission width was determined according to the time dependence formulation used in ABLA and the transient time from the expressions proposed by Bhatt and collaborators in Ref. [6].

The calculations reported in Fig. 13 clearly show the expected decrease of the fission lifetime with energy (solid

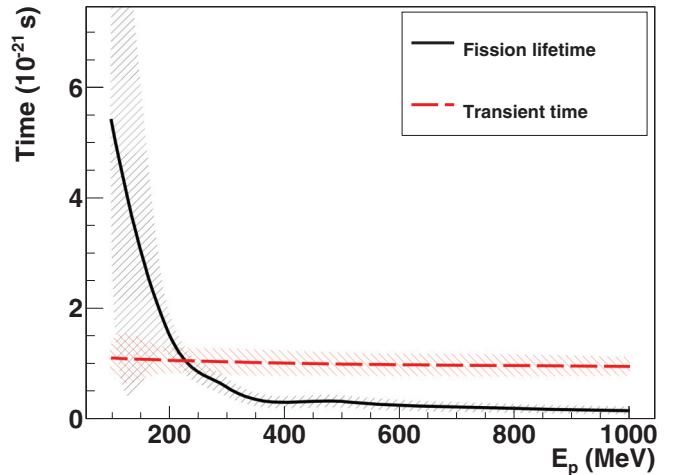


FIG. 13. (Color online) Average fission lifetime (solid line) compared to the corresponding average transient time (dashed line) as a function of the proton energy for the reaction $^{181}\text{Ta} + p$. The shaded area represents the time dispersion induced in both cases by the different temperatures and fission barriers of the fissioning nuclei.

line) and an almost constant value of the transient time (dashed line). From the evolution of these curves one can conclude that at low energies fission times are dominated by phase-space effects and only at proton kinetic energies above 250 MeV (around 100 MeV of excitation energy) do transient effects influence the fission probability.

The dependence of the reduced viscosity parameter β on temperature is another controversial subject. Several works have pointed out the need of relatively strong temperature-dependent viscosity parameter to explain pre-scission GDR γ -ray emission [18,75] or pre-scission neutron multiplicities [76] at excitation energies above 40 MeV. However, according to Lestone and McCalla [58] the deduced temperature dependence of the viscosity parameter is produced by an inadequate description of the fission widths in the calculations performed in these works.

Our data cover a large range in excitation energy, from about 100 to 500 MeV, and as shown in Fig. 12 all fission cross sections can be rather well described with a constant value of the dissipation strength. Therefore, we can conclude that we do not observe any sizable dependence of the dissipation parameter with temperature at small deformations within the limits of our experimental resolution. A similar conclusion was obtained from measurements in fragmentation reactions, also over a large range of excitation energy and fissioning systems [14,15]. These findings are supported by microscopic calculations showing a temperature dependence of the dissipation parameter below the present experimental resolution [19].

Finally, the fact that we can describe the fission of initially deformed nuclei ($\beta_2 = 0.269$) with the same viscosity parameter as for the nearly spherical systems investigated in Ref. [14] would suggest a weak or even a nonexistent dependence of the dissipation parameter with deformation within the range covered by this comparison.

VI. SUMMARY AND CONCLUSIONS

In this work, we have investigated the proton-induced fission of ^{181}Ta in inverse kinematics at 300, 500, 800, and 1000 A MeV. The combination of the inverse kinematics technique with a highly efficient detection setup made it possible to determine the total fission cross sections with high accuracy. The coincident measurement of both fission fragments and the rough determination of their atomic number from energy-loss measurements made it possible to unambiguously identify and separate the fission events from other reaction channels. This selection was shown to be extremely useful, in particular at the lower energies with rather small fission cross sections.

The new data have shed light on the energy region above 700 MeV, where only a few measurements with large uncertainties existed previously. At intermediate energies, the quality of the new data made it possible to clarify previous discrepant measurements. Moreover, these new data confirm the systematics established by Prokofiev over the entire energy range.

A comprehensive comparison of the experimental data with different state-of-the-art models describing fission was made to get a better insight into the dynamics of the fission process and benchmark the codes. The calculations have shown that different intranuclear cascade codes provide very similar results. However, deexcitation models based on a statistical description of the fission width provide rather discrepant results. These discrepancies seem to be associated to the different parametrizations used to describe the level-density parameters and to the different formalism used to describe particle evaporation. Moreover, statistical calculations using

realistic values for the level-density parameter overestimate the measured cross sections for the complete range of energies covered in this work.

Kramers-type calculations including dissipative but not transient effects only reproduce the fission cross sections for excitation energies below 100 MeV. At higher excitation energies fission cross sections are only described when presaddle transient effects are considered in a time-dependent fission decay width. These conclusions are supported by other works where the ABLA deexcitation code has been validated using other reactions and observables.

The onset of transient effects, for excitation energies above 100 MeV, is reproduced for a value of the reduced dissipation coefficient of $\beta = 4.5 \times 10^{21} \text{ s}^{-1}$, corresponding to a transient time of $\tau_f = 1.0 \pm 0.3 \times 10^{-21} \text{ s}$, in good agreement with other works. Moreover, the same value of the dissipation strength reproduces the fission cross sections for the complete range of energies measured in this work. This result would indicate that presaddle dissipative effects do not depend on temperature.

ACKNOWLEDGMENTS

This work was partially supported by the European Commission under Project No. FI6W-CT-2004-516520 EUROTRANS, by the Spanish Ministry of Research and Innovation under the Grants No. FPA2010-22174-C02-01 and No. BES-2008-005553, the project consolider-CPAN CSD2007-00042, and the Regional Government of Galicia under the program “grupos de referencia competitiva” 2006/46.

-
- [1] N. Bohr and J. A. Wheeler, *Phys. Rev.* **56**, 426 (1939).
 - [2] H. A. Kramers, *Physika VII* **4**, 284 (1940).
 - [3] P. Grangé, J.-Q. Li, and H. A. Weidenmüller, *Phys. Rev. C* **27**, 2063 (1983).
 - [4] B. Jurado, K.-H. Schmidt, and J. Benlliure, *Phys. Lett. B* **553**, 186 (2003).
 - [5] B. Jurado, C. Schmitt, K.-H. Schmidt, J. Benlliure, and A. R. Junghans, *Nucl. Phys. A* **747**, 14 (2005).
 - [6] K. H. Bhatt, P. Grangé, and B. Hiller, *Phys. Rev. C* **33**, 954 (1986).
 - [7] D. Hilscher and H. Rossner, *Ann. Phys. Fr.* **17**, 471 (1992).
 - [8] D. J. Hinde, D. Hilscher, H. Rossner, B. Gebauer, M. Lehmann, and M. Wilpert, *Phys. Rev. C* **45**, 1229 (1992).
 - [9] P. Paul and M. Thoennessen, *Annu. Rev. Nucl. Part. Sci.* **44**, 65 (1994).
 - [10] J. D. Molitoris *et al.*, *Phys. Rev. Lett.* **70**, 537 (1993).
 - [11] F. Goldenbaum *et al.*, *Phys. Rev. Lett.* **82**, 5012 (1999).
 - [12] P. Fröbrich and I. I. Gontchar, *Phys. Rep.* **292**, 131 (1998).
 - [13] D. Jacquet and M. Morjean, *Prog. Part. Nucl. Phys.* **63**, 155 (2009).
 - [14] C. Schmitt, K.-H. Schmidt, A. Kelić, A. Heinz, B. Jurado, and P. N. Nadtochy, *Phys. Rev. C* **81**, 064602 (2010).
 - [15] B. Jurado, C. Schmitt, K. H. Schmidt, J. Benlliure, T. Enqvist, A. R. Junghans, A. Kelic, and F. Rejmund, *Phys. Rev. Lett.* **93**, 072501 (2004).
 - [16] J. Benlliure, E. Casarejos, J. Pereira, and K.-H. Schmidt, *Phys. Rev. C* **74**, 014609 (2006).
 - [17] J. Benlliure *et al.*, *Nucl. Phys. A* **700**, 469 (2002).
 - [18] D. J. Hofman, B. B. Back, and P. Paul, *Phys. Rev. C* **51**, 2597 (1995).
 - [19] V. V. Sargsyan, Y. V. Palchikov, Z. Kanokov, G. G. Adamian, and N. V. Antonenko, *Phys. Rev. C* **76**, 064604 (2007).
 - [20] K. N. Clausen, in *Proceedings of the 16th Meeting of the International Collaboration on Advanced neutron Sources, ICANS-XVI*, edited by G. Mank and H. Conrad (Forschungszentrum Jülich GmbH, Jülich, Germany, 2003), Vol. 1, 2 & 3.
 - [21] H. Nifenecker, S. David, J. M. Loiseaux, and O. Meplan, *Nucl. Instrum. Methods Phys. Res., Sect. A* **463**, 42 (2001).
 - [22] <http://isolde.web.cern.ch/isolde/>.
 - [23] R. L. Burman and L. L. Daemen, *Nucl. Instrum. Methods Phys. Res., Sect. A* **370**, 335 (1996).
 - [24] B. Jurado, C. Schmitt, K.-H. Schmidt, J. Benlliure, and A. R. Junghans, *Nucl. Phys. A* **757**, 329 (2005).
 - [25] H. Delagrangé, G. Gregoire, F. Scheiter, and Y. Abe, *Z. Phys. A* **323**, 437 (1986).
 - [26] V. I. Yurevich, V.A. Nikolaev, R. M. Yakovlev, and I. B. Vorobiev, *J. Fiz. Elem. Chastits At. Yadra Lett.* **2**, 49 (2005).
 - [27] B. A. Bochagov, V. S. Bychenkov, V. D. Dmitriev, S. P. Mal'cev, A. I. Obukhov, N. A. Perfilov, V. A. Udod, and O. E. Shigaev, *Sov. J. Nucl. Phys.* **28**, 291 (1978).
 - [28] V. I. Baranovskiy, A. N. Murin, and B. K. Preobrazhenskiy, *Radiokhimiya* **4**, 470 (1962).

- [29] V. A. Konshin, *Sov. J. Nucl. Phys.* **2**, 489 (1966).
- [30] O. E. Shigaev, V. S. Bychenkov, M. F. Lomanov, A. I. Obukhov, N. A. Perfilov, G. G. Shimchuk, and R. M. Jakovlev, Report of the Khlopin Radium Institute, Leningrad Reports, 17, 1973.
- [31] M. Maurette and C. Stephan, in *Proceedings of IAEA Conference on Physics and Chemistry of Fission, Salzburg, Austria*, Vol. 2 (IAEA, Vienna, 1965), p. 307.
- [32] C. Stephan and M. L. Perlman, *Phys. Rev.* **164**, 1528 (1967).
- [33] B. Fernandez *et al.*, *Nucl. Phys. A* **747**, 227 (2005).
- [34] M. Bernas *et al.*, *Nucl. Phys. A* **725**, 213 (2003).
- [35] T. Enqvist *et al.*, *Nucl. Phys. A* **686**, 481 (2001).
- [36] J. Benlliure *et al.*, *Nucl. Phys. A* **683**, 513 (2001).
- [37] J. Pereira *et al.*, *Phys. Rev. C* **75**, 014602 (2007).
- [38] K. H. Schmidt *et al.*, *Nucl. Phys. A* **665**, 221 (2000).
- [39] M. Pfützner *et al.*, *Nucl. Instrum. Methods B* **86**, 213 (1994).
- [40] P. J. Karol, *Phys. Rev. C* **11**, 1203 (1975).
- [41] B. D. Wilkins, E. P. Steinberg, and R. R. Chasman, *Phys. Rev. C* **14**, 1832 (1976).
- [42] A. V. Prokofiev, *Nucl. Instrum. Methods Phys. Res., Sect. A* **463**, 557 (2001).
- [43] J. Cugnon, C. Volant, and S. Vuillier, *Nucl. Phys. A* **620**, 475 (1997).
- [44] X. Wang, J. Rapaport, M. Palarczyk, C. Hautala, X. Yang, D. L. Prout, B. Anderson, A. R. Baldwin, J. Olmsted, J. W. Watson, W.-M. Zhang, I. VanHeerden, E. J. Stephenson, R. Howes, S. Parks, E. Sugarbaker, B. A. Brown, and F. Sammarruca, *Phys. Rev. C* **66**, 014606 (2002).
- [45] Y. Yariv and Z. Fraenkel, *Phys. Rev. C* **20**, 2227 (1979).
- [46] L. G. Moretto, *Nucl. Phys. A* **247**, 211 (1975).
- [47] A. Kelic, M. V. Ricciardi, and K.-H. Schmidt, in *Proceedings of Joint ICTP-IAEA Advanced Workshop on Model Codes for Spallation Reactions, ICTP Trieste, Italy, 4–8 February (2008)*, edited by D. Filges, S. Leray, Y. Yariv, A. Mengoni, A. Stanculescu, and G. Mank (IAEA, Vienna, 2008), INDC(NDS)-530, p. 181–221.
- [48] R. Charity *et al.*, *Nucl. Phys. A* **483**, 371 (1988).
- [49] V. Weisskopf, *Phys. Rev.* **52**, 295 (1937).
- [50] C. Schmitt *et al.*, *Int. J. Mod. Phys. E* **18**, 2150 (2009).
- [51] W. Ye and N. Wang, *Phys. Rev. C* **87**, 014610 (2013).
- [52] S. G. McCalla and J. P. Lestone, *Phys. Rev. Lett.* **101**, 032702 (2008).
- [53] J. Töke and W. J. Swiatecki, *Nucl. Phys. A* **372**, 141 (1981).
- [54] W. Reisdorf, *Z. Phys. A* **300**, 227 (1981).
- [55] A. R. Junghans, M. de Jong, H.-G. Clerc, A. V. Ignatyuk, G. A. Kudyaev, and K.-H. Schmidt, *Nucl. Phys. A* **629**, 635 (1998).
- [56] J. R. Huizenga and L. G. Moretto, *Annu. Rev. Nucl. Sci.* **22**, 427 (1972).
- [57] A. V. Ignatyuk *et al.*, *Sov. J. Nucl. Phys.* **21**, 612 (1975).
- [58] J. P. Lestone and S. G. McCalla, *Phys. Rev. C* **79**, 044611 (2009).
- [59] V. M. Strutinsky, *Phys. Lett. B* **47**, 121 (1973).
- [60] K. H. Schmidt, *Int. Mod. Phys. E* **18**, 850 (2009).
- [61] A. J. Sierk, *Phys. Rev. C* **33**, 2039 (1986).
- [62] P. Möller *et al.*, *At. Data Nucl. Data Tables* **59**, 185 (1995).
- [63] M. V. Ricciardi *et al.*, *Phys. Rev. Lett.* **90**, 212302 (2003).
- [64] J. B. Natowitz *et al.*, *Phys. Rev. C* **65**, 034618 (2002).
- [65] D. Mancusi, R. J. Charity, and J. Cugnon, *Phys. Rev. C* **82**, 044610 (2010).
- [66] W. Hauser and H. Feshbach, *Phys. Rev.* **87**, 366 (1952).
- [67] M. V. Ricciardi *et al.*, *Phys. Rev. C* **73**, 014607 (2006).
- [68] W. Ye and N. Wang, *Phys. Rev. C* **86**, 034605 (2012).
- [69] A. Gavron *et al.*, *Phys. Rev. C* **35**, 579 (1987).
- [70] N. P. Shaw *et al.*, *Phys. Rev. C* **61**, 044612 (2000).
- [71] P. Grangé, S. Hassani, H. A. Weidenmüller, A. Gavron, J. R. Nix, and A. J. Sierk, *Phys. Rev. C* **34**, 209 (1986).
- [72] K. Siwek-Wilczynska, I. Skwira, and J. Wilczynski, *Phys. Rev. C* **72**, 034605 (2005).
- [73] M. Thoennessen and G. F. Bertsch, *Phys. Rev. Lett.* **71**, 4303 (1993).
- [74] L. G. Moretto, K. X. Jing, R. Gatti, G. J. Wozniak, and R. P. Schmitt, *Phys. Rev. Lett.* **75**, 4186 (1995).
- [75] I. Dioszegi, N. P. Shaw, I. Mazumdar, A. Hatzikoutelis, and P. Paul, *Phys. Rev. C* **61**, 024613 (2000).
- [76] J. Wilczynski, K. Siwek-Wilczynska, and H. W. Wilschut, *Phys. Rev. C* **54**, 325 (1996).